Bioactive Materials 24 (2023) 438–449

Contents lists available at ScienceDirect

Bioactive Materials

journal homepage: www.keaipublishing.com/en/journals/bioactive-materials

Click and bioorthogonal hyaluronic acid hydrogels as an ultra-tunable platform for the investigation of cell-material interactions

Nathan Lagneau, Pierre Tournier, Boris Halgand, François Loll, Yves Maugars, Jérôme Guicheux, Catherine Le Visage, Vianney Delplace *

Nantes Université, Oniris, CHU Nantes, INSERM, Regenerative Medicine and Skeleton, RMeS, UMR 1229, F-44000, France

ARTICLE INFO

Keywords:
Hydrogels
Click and bioorthogonal chemistry
Hyaluronic acid
Mesenchymal stromal cells
Cell-material interactions
Secretome

ABSTRACT

The cellular microenvironment plays a major role in the biological functions of cells. Thus, biomaterials, especially hydrogels, which can be design to mimic the cellular microenvironment, are being increasingly used for cell encapsulation, delivery, and 3D culture, with the hope of controlling cell functions. Yet, much remains to be understood about the effects of cell-material interactions, and advanced synthetic strategies need to be developed to independently control the mechanical and biochemical properties of hydrogels. To address this challenge, we designed a new hyaluronic acid (HA)-based hydrogel platform using a click and bioorthogonal strain-promoted azide-alkyne cycloaddition (SPAAC) reaction. This approach facilitates the synthesis of hydrogels that are easy to synthesize and sterilize, have minimal swelling, are stable long term, and are cytocompatible. It provides bioorthogonal HA gels over an uncommonly large range of stiffness (0.5–45 kPa), all forming within 1–15 min. More importantly, our approach offers a versatile one-pot procedure to independently tune the hydrogel composition (e.g., polymer and adhesive peptides). Using this platform, we investigate the independent effects of polymer type, stiffness, and adhesion on the secretory properties of human adipose-derived stromal cells (hASCs) and demonstrate that HA can enhance the secretion of immunomodulatory factors by hASCs.

1. Introduction

Using synthetic biomaterials to study cell-material interactions is a booming area of research. Over the past decade, extensive work has been dedicated to deciphering the role of the extracellular matrix (ECM) in cell behavior using synthetic materials as model ECMs. These investigations rapidly evolved from 2D to more representative 3D interactions thanks to the development of new generations of cell-friendly materials. In particular, innovative hydrogels have attracted increasing attention because of their ability to recapitulate the hydrated nature, composition, and mechanical properties of natural ECM. Yet, independently tuning the physicochemical and biochemical properties of cytocompatible hydrogels remains a challenge. Consequently, while the influence of mechanical properties (e.g., stiffness), which are the easiest to tune from a material perspective, have been largely studied [1–3], much work remains to be done on the effect of biochemical cues (e.g., polymer composition and biomimetic peptides) on cell behavior. More importantly, the influence of these parameters is often questioned separately due to the limited tunability of existing systems, impairing our ability to screen and combine desired conditions. Thus, building a new hydrogel platform to investigate cell-material interactions would require combining ease of synthesis, sterilizability, and a customizable range of gelation time with features necessary for 3D cell culture (e.g., cytocompatibility, absence of swelling, and long-term stability) with independently tunable mechanical and biochemical properties.

When developing a new hydrogel platform, hyaluronic acid (HA) is particularly relevant because it is a natural component of the ECM, commercially available and affordable, and is relatively easy to chemically modify [4,5]. However, most common HA crosslinking strategies require multiple and complex synthetic steps [6], and external stimuli or small molecule reagents that are not entirely compatible with physiological conditions [7,8], or have inherent limitations, such as poor mechanical properties and slow gelation rate [9]. To address these issues, researchers have been exploring new crosslinking strategies that follow two major chemistry concepts: click chemistry and bioorthogonality. Ideally, click reactions are reactions that are efficient under mild

Peer review under responsibility of KeAi Communications Co., Ltd.
* Corresponding author.
E-mail address: vianney.delplace@univ-nantes.fr (V. Delplace).

https://doi.org/10.1016/j.bioactmat.2022.12.022
Received 21 September 2022; Received in revised form 30 November 2022; Accepted 21 December 2022

conditions, and by extension, under physiological temperature and pH, and that do not produce byproducts, eliminating the need for purification [10]. Bioorthogonality refers to chemical reactions that do not alter, or are not altered by, biological components and biochemical processes [11,12]. Together, these two concepts encompass a short list of chemical reactions (e.g., Diels-Alder, inverse electron-demand Diels-Alder, and strain-promoted azide-alkyne cycloaddition [SPAAC]) that are considered ideal for hydrogel design [13]. However, most of the click and bioorthogonal reactions investigated to date produced hydrogels with inherent limitations such as a slow gelation rate (e.g., Diels-Alder) [14] or a limited range of mechanical properties (e.g., inverse electron-demand Diels-Alder) [15].

To our knowledge, there has been only one report of HA-only hydrogels that use SPAAC, where the authors used a complex synthetic route involving organic solvents and compounds that are not commercially available [16]. The resulting hydrogels had slow gelation rates, requiring high polymer content (>100 min for 1% [w/v] polymer content), with extremely limited stability in culture medium (<4 days). Other groups combined HA and PEG crosslinkers in various SPAAC-based strategies, however, these strategies required the use of high molecular weight HA (2 MDa) [17], which is difficult to sterilize, or high polymer content (10% [w/v]) [18], which typically increases the viscosity of hydrogel precursors, both leading to hydrogels with a limited range of stiffness (≈100–1000 Pa) and unwanted swelling [17–19]. HA-PEG crosslinking via SPAAC was also investigated for the development of an innovative bioprinting process, where a support bath composed of gelatin microbeads allowed the diffusion of a PEG crosslinker toward a printed polymer filament for spatially controlled gelation. Although extremely promising, this strategy required a rather long incubation of the construct under non-physiological conditions (several hours at 4 or 20 °C) to complete the crosslinking process [20]. Other polysaccharides, such as alginate or cellulose, have also been used as polymer backbones to synthesize SPAAC hydrogels, leading to hydrogels with limited mechanical properties or stability [21,22]. Therefore, designing a new HA-based hydrogel platform ideal for investigating cell-material interactions required a new click and bioorthogonal crosslinking strategy.

In this study, we investigated the use of the SPAAC chemistry between a cyclooctyne and an azide as a click and bioorthogonal crosslinking mechanism to synthesize tunable HA hydrogels (Fig. 1). We successfully functionalized HA with either a cyclooctyne (bicyclononyne, BCN) or an azide (N_3) via a single-step synthesis and obtained HA-only hydrogels that form within minutes at low polymer content. By carefully investigating the influence of the crosslinking density on the hydrogel properties, we were able to design a variety of fast-forming and stable HA hydrogels over a large range of stiffness (0.5–45 kPa), including gels with minimal to no swelling (0.5–5 kPa). We demonstrated the cytocompatibility (>95% viable cells after 7 days) and use of these new HA hydrogels for 3D cell culture using L929 murine fibroblast cells and human adipose-derived stromal cells (hASCs). We also showed that, independent of a chosen stiffness, the composition of SPAAC HA-based hydrogels can be tuned by immobilizing biomimetic peptides or co-crosslinking additional glycosaminoglycans (e.g., chondroitin sulfate), making these hydrogels a versatile platform to investigate cell-material interactions. Moreover, to demonstrate the usefulness of this platform, we investigated how the composition and stiffness of the hydrogels influence the secretions of encapsulated hASCs, which are central to their use as therapeutic cells [23,24]. Our results showed that HA advantageously increases the secretion of a series of immunomodulatory factors by hASCs cultured under pro-inflammatory conditions, paving the way for new cell-material investigations and the potential development of next-generation, material-assisted cell therapies.

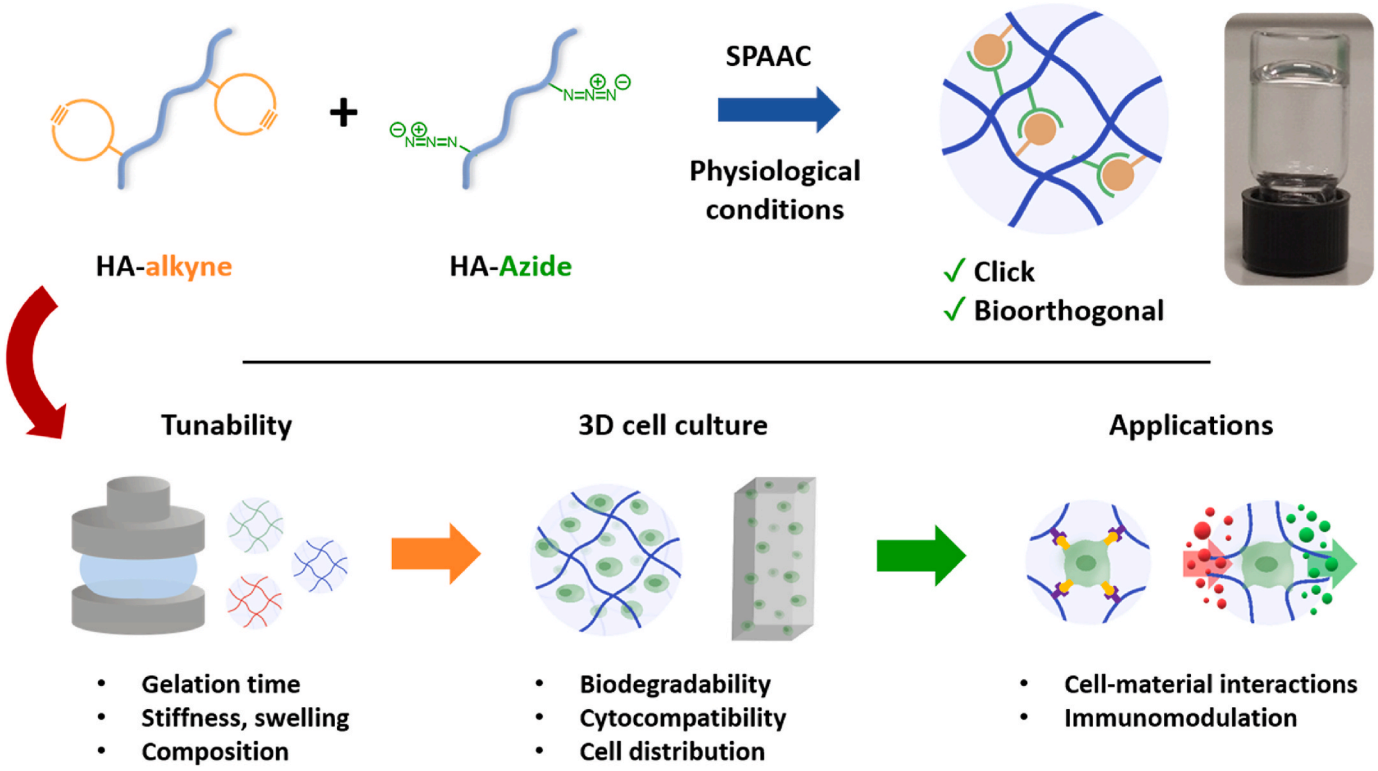

Fig. 1. Designing ultra-tunable hyaluronic acid (HA)-based hydrogels via strain-promoted azide-alkyne cycloaddition (SPAAC) crosslinking for the investigation of cell-material interactions. In this study, we investigated the tunability and cytocompatibility of a new click and bioorthogonal HA hydrogel platform and demonstrated its use for investigating the effects of cell-material interactions on stem cell immunomodulatory properties.

2. Experimental section/methods

2.1. Materials

Sodium hyaluronate was purchased from Lifecore Biomedical (USA). Chondroitin sulfate C sodium salt (CS) was purchased from Carbosynth (USA). Alginate (Protanal LF10/60) was purchased from FMC Corporation (USA). 2-(N-morpholino)ethanesulfonic acid (MES) and 4-(4,6-dimethoxy-1,3,5-triazin-2-yl)-4-methylmorpholinium chloride (DMT-MM) were purchased from TCI Chemicals (Belgium). Azido-PEG2-amine was purchased from Broadpharm (USA). Dulbecco's Phosphate Buffered Saline (without Ca & Mg), Dulbecco's Modified Eagle Medium (DMEM), Penicillin/Streptomycin (P/S), Alexa Fluor 568 phalloidin, Hoechst 33258, and the Live/Dead Kit were purchased from ThermoFischer Scientific. L929 cells were purchased from ATCC (USA). Fetal Bovine serum (FBS) was purchased from Dominique Dutscher. Otherwise stated, all other reagents were purchased from Sigma-Aldrich.

2.2. Methods

2.2.1. Polysaccharide modification

Synthesis of HA-N_3: HA-N_3 was synthesized by adapting a previously described protocol [15]. Typically, HA (100 mg) with various molecular weights (100 kDa and 300 kDa) was dissolved in MES buffer pH 5.5 (9 mL) at room temperature while stirring. DMT-MM (0.69 mg; 1 eq) was added and allowed to react for 30 min. Then, azido-PEG2-amine (22 mg; 0.5 eq) was dissolved in MES buffer pH 5.5 (1 mL), added dropwise to the polymer solution, and allowed to react for 3 days at room temperature while stirring. To tune the DS, a similar procedure was followed with adjusted equivalents of DMT-MM (34 mg; 0.5 eq) and azido-PEG2-amine (11 mg; 0.25 eq). The solution was dialyzed against 0.1 M DPBS for 1 day, then against deionized water for 2 days, before filter sterilization, lyophilization, and storage at −20 °C. The DS of HA-N_3 was determined using ^{1}H NMR (400 MHz, D_2O): after subtracting the signals from unmodified HA between 3.1 ppm and 4.4 ppm, the 3 protons of the N-acetyl group of HA (2.1 ppm) served as a reference to calculate the relative amount of grafted N_3 (13 protons between 3.3 and 4.1 ppm). CS-N_3 and alginate-N_3 were functionalized and characterized using the same procedure.

Synthesis of HA-BCN: HA-BCN was synthesized as described above with some modifications. HA (100 mg) with various molecular weights (100 kDa and 300 kDa) was dissolved in MES buffer pH 5.5 (9 mL) at room temperature while stirring. DMT-MM (27 mg; 0.4eq) was added and allowed to react for 30 min. BCN (16 mg; 0.2eq) was dissolved in DMSO (1 mL) prior to dropwise addition. The solution was allowed to react for 3 days at room temperature while stirring. To tune the DS, a similar procedure was followed with adjusted equivalents of DMT-MM (14 mg; 0.2 eq) and BCN (8 mg; 0.1 eq). The solution was dialyzed against 0.1 M DPBS containing 2% DMSO overnight, 0.1 M DPBS for 8 h, and deionized water for 2 days, prior to filter sterilization, lyophilization, and storage at −80 °C. The DS of HA-BCN was determined by ^{1}H NMR (400 MHz, D_2O): the 3 protons of the N-acetyl group of HA (2.1 ppm) served as a reference to calculate the relative amount of grafted BCN (2 protons at 1.1 ppm, 2 protons at 2.4 ppm, and 2 protons at 4.3 ppm). CS-BCN and alginate-BCN were functionalized and characterized using the same procedure.

Synthesis of fluorescent CS: CS or CS-N_3 was functionalized with a fluorophore using a procedure similar to that described in section 4.2.1. Polysaccharide modification. Briefly, the polymer (50 mg) was dissolved in MES buffer pH 5.5 (4.5 mL) at room temperature while stirring. DMT-MM (3 mg) was added and allowed to react for 30 min. Alexa Fluor™ 488 hydrazide (0.5 mg) was dissolved in DMSO (0.5 mL) prior to dropwise addition. The solution was allowed to react for 3 days in the dark at room temperature while stirring. The solution was dialyzed against 0.1 M DPBS containing 2% DMSO overnight, then 0.1 M DPBS for 8 h, and deionized water for 2 days, prior to filter sterilization, lyophilization, and storage at −20 °C.

2.2.2. Hydrogel formation and characterization

Hydrogel formation: Hydrogels were obtained by separately dissolving HA-BCN and HA-N_3 in the desired medium (e.g., PBS or DMEM with serum), prior to mixing them together in a chosen volume ratio. The initial concentrations and volume ratios of the two components were calculated to control both the final total concentration of polysaccharides and the BCN:N_3 molar ratio. For direct comparison, hydrogels with distinct DS or distinct MW but similar crosslinking densities (1.4 mM) were obtained by adjusting the polymer content and/or the BCN:N_3 molar ratio.

Gelation time evaluation: Rheological characterization was performed using a HAAKE™ MARS™ (ThermoFisher Scientific) equipped with a 20-mm titanium upper plate and a Peltier plate to control the temperature. All oscillatory time sweep experiments were performed at a constant stress of 1 Pa and at a constant frequency of 0.1 Hz (within the linear viscoelastic region). Pre-hydrogel solutions were prepared as described in section 4.2.2. Hydrogel formation and characterization, and measurements were performed immediately after mixing the hydrogel precursors. Gelation time experiments were conducted at 37 °C with a solvent trap to prevent evaporation. Gel points were determined as the time when the shear storage modulus (G′) value equals that of the shear loss modulus (G″).

Viscosity evaluation: Viscosity characterization was performed using a HAAKE™ MARS™ (ThermoFisher Scientific) equipped with a 35-mm 1° titanium upper cone and a Peltier plate to control the temperature. Viscosity measurements of HA solutions were performed at 37 °C in a shear rate range of 0.1–1000 s^{-1}. Flow curves were fitted using the simplified Cross model to determine the zero-shear viscosity values (η0).

Stiffness evaluation: A volume of 200 μL of pre-hydrogel solution was cast between two glass plates separated by a 1-mm silicon spacer and left at 37 °C overnight in a humid atmosphere for complete gelation. Hydrogels were then punched (2 mm in diameter) and subjected to unconfined compression tests using a Microtester® (CellScale), with measurements performed under 20% strain. Young's modulus was calculated according to the manufacturer recommendations and the standard expression: $= \frac{stress}{strain} = \frac{F/A}{\Delta I/I_0}$, where E is the Young's modulus; F, the force applied to the gel; A, the area on which the force is applied; ΔI, the displacement, and I_0, the initial thickness. For each formulation, 3 distinct hydrogels were prepared and punched in at least 4 locations.

Stability and biodegradability studies: 200 μL of various pre-hydrogel solutions were transferred to pre-weighted Eppendorf tubes and left at 37 °C overnight for complete gelation. The hydrogel-containing tubes were weighed, and 800 μL of PBS (37 °C) was added. At specific time points (0, 1, 2, 4, 6, and 24 h; then 3, 7, 14, 21, 42, and 63 days), the supernatant was removed before weighing the hydrogel. A biodegradability study was then conducted on three formulations of interest for their stability by adding 800 μL of hyaluronidase (100 U mL^{-1} in PBS; 37 °C) on top of the stable hydrogels. The three formulations investigated were the following: (i) 1 kPa HA hydrogel (1% HA w/v; DS: HA-BCN, 15%; HA-N_3, 40%; BCN:N_3 ratio of 4:1); (ii) 2.5 kPa HA hydrogel (1% HA (w/v); DS: HA-BCN, 15%; HA-N_3, 40%; BCN:N_3 ratio of 1:4); and (iii) 5 kPa HA hydrogel (1.5% HA (w/v); DS: HA-BCN, 7%; HA-N_3, 40%; BCN:N_3 ratio of 1:1). At specific time points (0, 2, 6, and 24 h; then 2, 3, 4, and 7 days), the supernatant was removed before weighing the hydrogel. The reported mass ratio represents the hydrogel mass at a specific time point divided by its initial mass.

Polymer switching: The four formulations investigated were the following: (i) 1 kPa HA hydrogel (1% HA [w/v]; DS: HA-BCN, 15%; HA-N_3, 40%; BCN:N_3 ratio of 4:1), (ii) 3 kPa HA hydrogel (1% HA [w/v]; DS: HA-BCN, 15%; HA-N_3, 40%; BCN:N_3 ratio of 1:4), (iii) 1 kPa Alginate hydrogel (0.5% alginate [w/v]; DS: alginate-BCN, 8%; HA-N_3, 30%; BCN:N_3 ratio of 1:1), (iv) 3 kPa Alginate hydrogel (1% alginate [w/v]; DS: alginate-BCN, 15%; HA-N_3, 40%; BCN:N_3 ratio of 1:1).

GAG enrichment evaluation: Fluorescent CS or fluorescent CS-N_3 was dissolved at 0.1% (w/v) in PBS. Then, HA-N_3 was dissolved at 1% (w/v) in PBS containing either fluorescent CS or fluorescent CS-N_3. Each of the two HA-N_3 solutions were mixed with a 1% (w/v) HA-BCN solution in a volume ratio corresponding to an HA-BCN:HA-N_3 molar ratio of 4:1. 100 μL of the forming HA gels containing either fluorescent CS or fluorescent CS-N_3 were transferred to a 96-well plate and allowed to gel overnight at room temperature. 100 μL of PBS was added on top of each fluorescent hydrogel before monitoring fluorescent CS release: at specific time points (0, 2, 8, and 24 h; then 3 and 7 days), the supernatant was removed and the fluorescence of both the hydrogel and the supernatant was measured (Ex: 485 nm, Em: 535 nm; Tristar 2 S plate reader, Berthold Technologies). The results were normalized to the initial hydrogel fluorescence.

2.2.3. Biological investigations

Cell culture and encapsulation: Murine fibroblastic L929 cells were amplified in DMEM medium supplemented with 10% FBS and 1% P/S. As previously described [25], hASCs were isolated from lipoaspirates of patients with their informed consent and amplified in Promocell growth medium supplemented with 1% P/S. hASCs were used between passage 2 and 5. For cell encapsulation, HA-BCN and HA-N_3 were first dissolved in DMEM medium supplemented with 10% FBS and 1% P/S. Cells were then pelleted and resuspended in the HA-N_3 solution. The solutions of HA-BCN and HA-N_3/cells were mixed in a calculated volume ratio to obtain the desired total HA concentration (1% w/v), the desired BCN:N_3 molar ratio (1:4), and a final cell concentration of 10^6 cells/mL. Cell-containing pre-hydrogel solutions (100 μL) were rapidly transferred to inserts (8 μm pore; Sarstedt) and allowed to gel for 30 min at 37 °C before adding cell medium. The medium was changed every 2–3 days.

Viability and metabolic assays: Cell viability and metabolic activity were assessed at day 0, 3, and 7 using LIVE/DEAD™ staining and the CCK-8 assay, respectively. For LIVE/DEAD™ staining, gels were transferred to an 8-well chamber slide (IBIDI) and incubated with Calcein AM and ethidium homodimer per the manufacturer's recommendations. Images were acquired via confocal microscopy (A1RS, Nikon). Cell viability was calculated as the number of living cells divided by the total number of cells. Cell distribution was calculated as the number of cells per 125 μm gel section divided by the total cell number in a 500 μm volume of gel. Regarding the metabolic activity assay, gels were transferred to a 48-well plate and incubated for 2 h with a CCK-8 solution per the manufacturer's recommendations. The absorbance of the supernatant at 460 nm was measured (Tristar 2 S plate reader, Berthold Technologies), and the results were normalized to the absorbance measured on D0. The viability and metabolic activity experiments were performed on 3 distinct batches of polymers (i.e., HA-BCN and HA-N_3).

One-pot peptide immobilization: HA-BCN, HA-N_3, and the RGD-N_3 peptide (N_3-KGSGSGRGDSP; GenScript) were first dissolved in DMEM medium supplemented with 10% FBS and 1% P/S. The solutions of HA-BCN and RGD-N_3 were mixed and allowed to react for 30 min at 37 °C. The solutions of HA-BCN (with or without RGD-N_3) and HA-N_3 were mixed in a calculated volume ratio to obtain the desired total HA concentration (1% w/v) and the desired BCN:N_3 molar ratio (4:1). 200 μL of the RGD-containing pre-hydrogel solutions were rapidly transferred to a 24-well plate and allowed to gel for 30 min at 37 °C before cell seeding (30 000 hASCs/well) on top of the hydrogel. After 1 day of cell culture, hydrogels were washed with PBS to remove non-adherent cells, then fixed with 4% paraformaldehyde and permeabilized with 0.1% Triton X-100. Cells were then labeled with Alexa Fluor 568 phalloidin (dilution of 1:200) and Hoechst 33258 (dilution of 1:50 000). Images of cells adhering to the gels were acquired using confocal imaging (A1RS, Nikon), prior to adhesion quantification expressed as number of nuclei per cm^2.

Evaluation of hASC secretions: hASCs were amplified before FBS deprivation overnight and encapsulated as described in section 2.2.3. Biological investigations. Cells were encapsulated in one of the five following formulations: (i) 1 kPa HA hydrogel (1% HA (w/v); DS: HA-BCN, 15%; HA-N_3, 40%; BCN:N_3 ratio of 4:1); (ii) 5 kPa HA hydrogel (1.5% HA (w/v); DS: HA-BCN, 7%; HA-N_3, 40%; BCN:N_3 ratio of 1:1); (iii) 1 kPa RGD HA hydrogel (1% HA (w/v); DS: HA-BCN, 15%; HA-N_3, 40%; BCN:N_3 ratio of 4:1; RGD-N_3: 300 μM); (iv) 1 kPa CS HA hydrogel (1% HA (w/v); DS: HA-BCN, 15%; HA-N_3, 40%; BCN:N_3 ratio of 4:1; CS-N_3: 0.1%); or (v) 1 kPa alginate hydrogel (0.5% alginate (w/v); DS: alginate-BCN, 8%; alginate-N_3, 30%; BCN:N_3 ratio of 1:1). 100 μL of the cell-containing pre-hydrogel solutions were rapidly transferred to a 96-well plate and allowed to gel for 30 min at 37 °C. The gels were then transferred to a 48-well plate before adding culture medium. After 4 h, the medium was removed, and cells were stimulated with medium containing 50 ng/mL of human tumor necrosis factor-α (TNF-α) and human interferon-γ (INF-γ) (Miltenyi Biotec). After 3 days of stimulation, the release of soluble factors in the supernatant was evaluated. The presence of indoleamine-2,3-dioxygenase (IDO) in the supernatant was evaluated based on the measurement of its enzymatic activity (i.e., tryptophan-to-kynurenine conversion) using an Ehrlich test as previously described [26]. The Prostaglandin E2 (PGE2) content was evaluated using an ELISA kit (Cayman Chemical) following the manufacturer's instructions. The level of interleukin-6 (IL-6) was evaluated using an ELISA kit (DuoSet®, R&D Systems) following the manufacturer's instructions.

2.3. Statistical analysis

All data are shown as mean ± standard deviation. Statistical analysis was carried out using GraphPad to evaluate statistical significance via Student's t-test or one-way ANOVA with Tukey's post hoc test.

3. Results and discussion

3.1. SPAAC hydrogel components can be synthesized in a single step

We hypothesized that SPAAC chemical reagents (i.e., strained cycloalkyne and azide) could be advantageously combined with HA for the design of click and bioorthogonal HA hydrogels that are easy to synthesize, tune, and use for 3D cell culture. Regarding the cyclooctyne, we chose to investigate the use of the Bicyclo[6.1.0]nonyne (BCN) over the commonly used dibenzocyclooctyne (DBCO) for its higher hydrophilicity and good balance between stability and reactivity [27]. For ease of use, the synthetic route of hydrogel precursors must be accessible and straightforward, with limited use of organic solvents and few synthetic/purification steps. Here, the two HA hydrogel components, namely HA-BCN and HA-N_3, were each synthesized in a single step using commercially available compounds via a standard amidation procedure (i.e., DMT-MM activation) under mild aqueous conditions of reaction and purification (Fig. 2a). Low to average HA MWs (20–300 kDa) were chosen to allow filter sterilization without polymer loss, thus enabling straightforward precursor sterilization. We successfully synthesized HA-BCN and HA-N_3 as confirmed by ^{1}H NMR (Fig. 2b), with high yields (>90%). More importantly, adjusting reagent equivalents allowed us to tune the degree of substitution (DS) of each functional group, from 7% ± 1%–15% ± 1% for HA-BCN, and from 21% ± 2%–40% ± 3% for HA-N_3 (Fig. 2c). Relatively low DS were targeted for BCN grafting due to the relative water solubility of the cyclooctyne, which could hamper filter sterilization for any DS > 20%. Interestingly, the use of DMT-MM as a coupling agent allowed us to obtain a higher BCN substitution yield (≥70%) than previously reported with the commonly used EDC reagent (≈25%) [28]. The synthesis of HA-N_3 and HA-BCN had good batch-to-batch reproducibility and could be applied over a range of MWs (from 100 to 300 kDa) without differences in substitution (Fig. S1). This range of MWs allows for filter sterilization, ensuring the synthesized polymers can be easily sterilized. Overall, we showed that the proposed strategy for the synthesis of SPAAC hydrogel precursors follows green chemistry principles (e.g., aqueous conditions, room temperature,

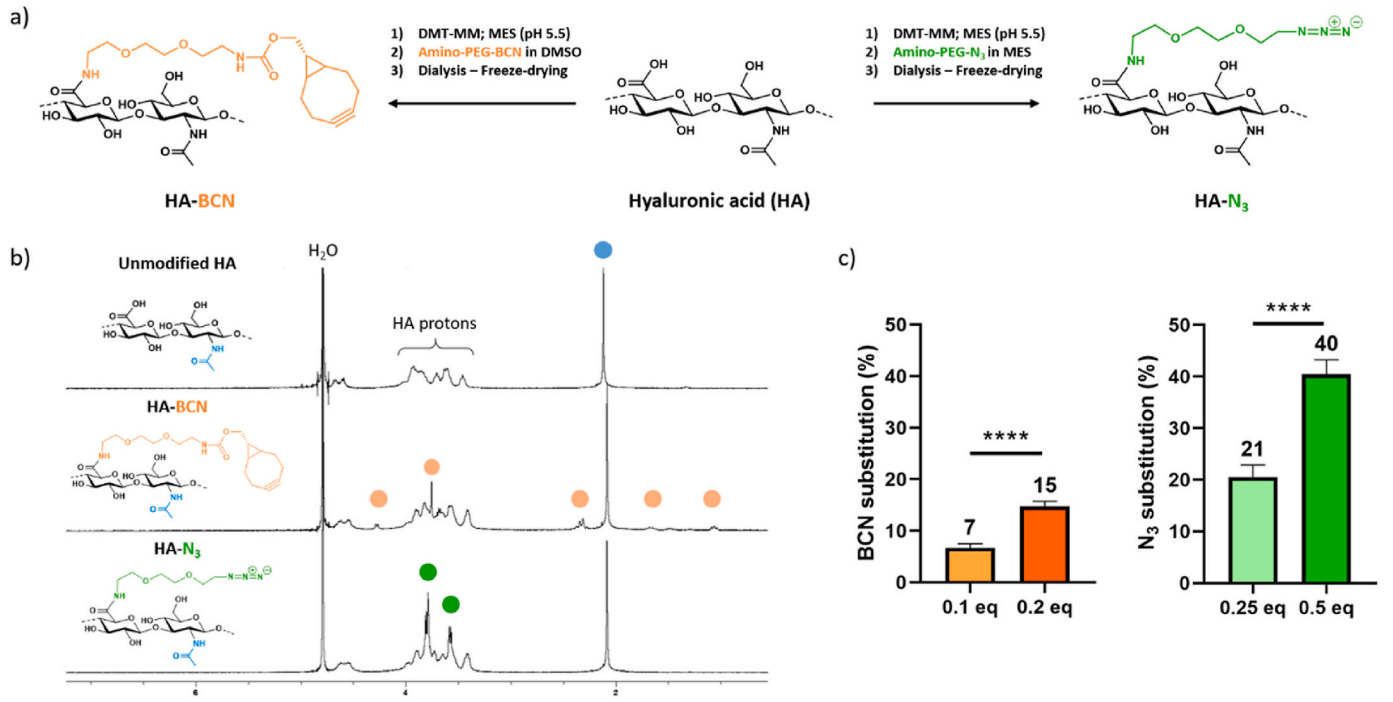

Fig. 2. Single-step synthesis of SPAAC precursors for the design of HA-based hydrogels. a) Single-step reaction conditions used for the synthesis of bicyclonyne (BCN)-modified and azide (N_3)-modified HA. b) Representative ^{1}H NMR (400 MHz, D_2O) of HA, HA-BCN, and HA-N_3 confirming the successful chemical modification of HA. The 3 protons of the N-acetyl group of HA (blue circle, 2.1 ppm) served as a reference to calculate the degrees of substitution of HA-BCN (orange circles, including 2 protons at 1.1 ppm, 2 protons at 2.4 ppm, and 2 protons at 4.3 ppm) and HA-N_3 (green circles, accounting for 13 protons between 3.3 and 4.1 ppm). c) Tunable degrees of substitution of HA-BCN and HA-N_3 using defined reagent equivalents. Data are shown as mean ± SD (N = 3 distinct polymer batches) with statistical significance determined by Student's t-test (****$p < 0.0001$).

single-step reactions, efficiency, and safety) and is reproducible and easy to implement, making it broadly applicable.

3.2. SPAAC hydrogels are fast gelling and offer a broad range of stiffness

Controlling the gelation kinetics of a gel is key to its broad application. For 3D cell culture, a relatively fast gelation (<10 min) is required to prevent cell sedimentation [15], yet a quasi-instantaneous gelation (<1 min) is not practical and can lead to inhomogeneous cell distribution. Gelation kinetics is related to the crosslinking reaction rate, the number of reactive functions per polymer chain, and the overall concentration of potential cross-links to be formed [29–31]. While the crosslinking reaction rate is determined by the reactivity of the chosen functional groups, the two other parameters can be adjusted by varying the polymer MW, DS, and content, as well as the molar ratio between reactive functions. Therefore, we carefully investigated the influence of these four variables on the gelation time of HA-based hydrogels formed via SPAAC. Of note, the overall concentration of potential cross-links is equivalent to the theoretical maximal crosslinking density. For simplicity, we will use the term "crosslinking density" throughout the text to designate both the concentration of potential cross-links (before gelation) and the theoretical maximal crosslinking density (after gelation). In the following experiments, we managed to compare hydrogels with similar crosslinking densities but either distinct DS or distinct MW by adjusting the polymer content and/or molar ratio between reactive functions. Using dynamic shear rheological measurements on 1% (w/v) HA gels (HA-BCN: DS of 7%; HA-N_3: DS of 40%) at a fixed crosslinking density (1.4 mM), we showed that increasing the MW of HA from 100 kDa to 300 kDa significantly reduced the gelation time from 8.8 ± 0.2 min to 3.1 ± 0.4 min (Fig. 3a). While the effect of polymer entanglement cannot be entirely excluded, these results mainly highlight the influence of the number of reactive groups per polymer chain on gelation kinetics, as previously observed [15,32]. To further confirm this result, we showed that increasing the DS of 100 kDa HA-BCN from 7% to 15% while keeping the crosslinking density (1.4 mM) constant significantly decreased the gelation time from 8.8 ± 0.2 min to 5.6 ± 0.2 min (Fig. 3b). These results highlight the advantage of working with tunable side-chain functionalized polymers over end-functionalized polymers, such as PEG, to tune the gelation time.

Following these experiments, we investigated the effects of the polymer content and the BCN:N_3 molar ratio, both of which are directly linked to the crosslinking density, on gelation time. As expected, we showed that the gelation time is strongly influenced by the polymer content, with an increase in overall modified HA concentration from 0.5% to 1.5% (w/v), leading to a decrease in gelation time from 10 ± 0.4 min to less than 1 min (Fig. 3c). Interestingly, we demonstrated that getting closer to a BCN:N_3 molar ratio of 1:1, which maximizes the crosslinking density, reduces the gelation time to a low of 2.8 ± 0.1 min for 1% (w/v) HA gels (HA-BCN: DS of 7%; HA-N_3: DS of 40%) (Fig. 3d). By plotting the gelation time of a large panel of hydrogel formulations as a function of their crosslinking densities, we further demonstrated that increasing the overall crosslinking density is key to reducing the gelation rate (Fig. 3e). More importantly, most of the formulations that we investigated gelled between 1 and 10 min, including some at ultra-low polymer content (typically 0.5% w/v), making SPAAC one of the fastest click crosslinking reactions ever reported for the synthesis of HA hydrogels. Overall, we identified formulations that offer a range of gelation times suitable for a variety of biomedical applications, including 3D cell culture [15].

While customizing the gelation time mainly serves a practical purpose, the stiffness of a gel has been shown to directly impact cell and tissue behaviors [1,2,33]. This makes stiffness an important parameter to control for the investigation of cell-material interactions. Thus, designing hydrogels that are tunable over a wide range of stiffness is desirable. The crosslinking density, which in this study is the density of junctions formed within a gel, is known to contribute to hydrogel

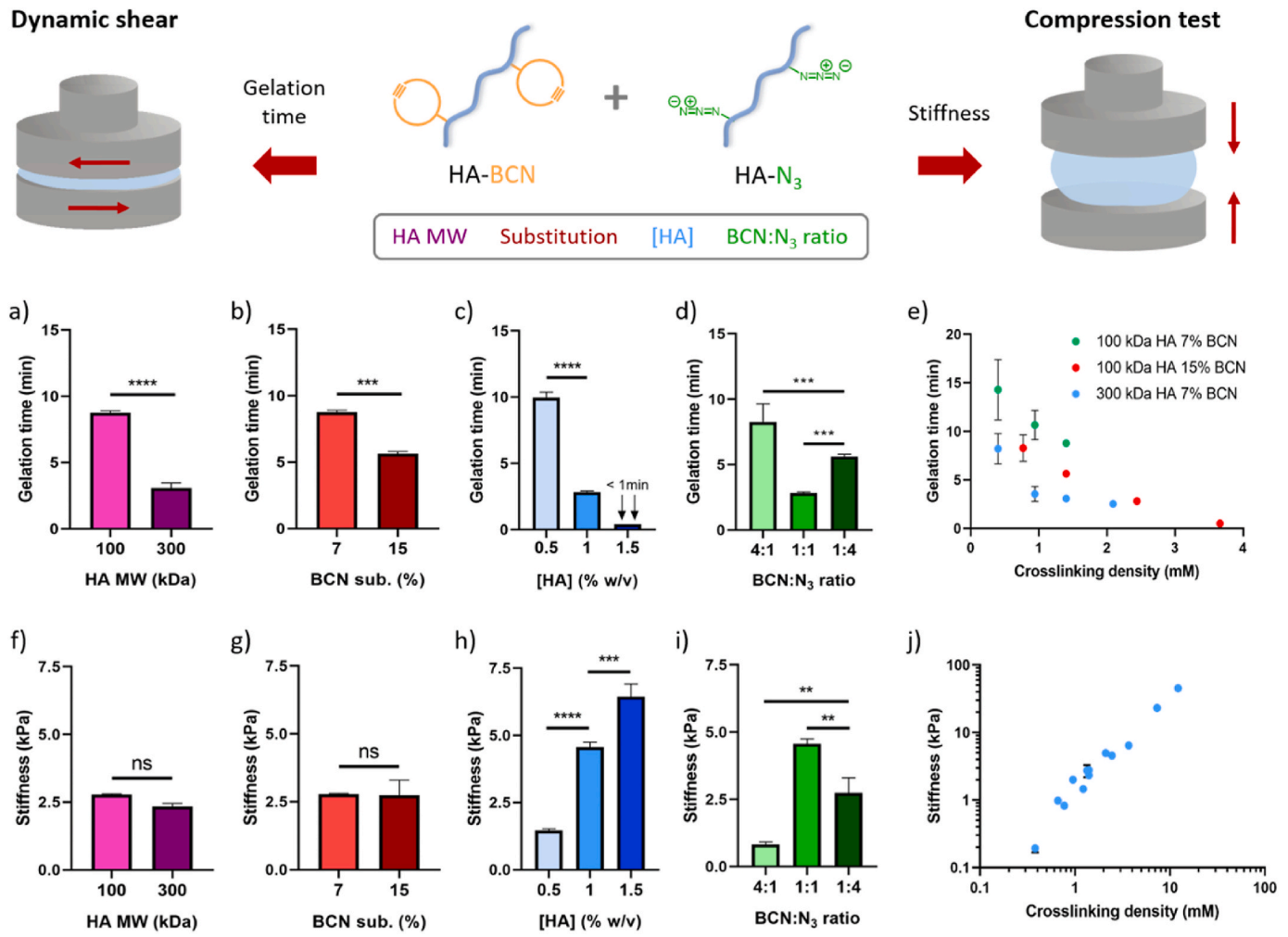

Fig. 3. Mechanical characterization of SPAAC HA-based hydrogels. The influence of a) HA MW, b) BCN DS, c) concentration of HA, and d) BCN:N_3 ratio on hydrogel gelation time, evaluated using dynamic shear rheometry. e) Relationship between hydrogel gelation time and crosslinking density, revealing the role of MW and crosslinking density on gelation kinetics. The influence of f) HA MW, g) BCN substitution, h) concentration of HA, and i) BCN:N_3 ratio on hydrogel stiffness, evaluated via compression testing. j) Overall plot of hydrogel stiffness vs crosslinking density, demonstrating a linear relationship. Data are shown as mean ± SD (n = 3) with statistical significance determined using Student's t-test or one-way ANOVA with a Tukey's post hoc test (ns: not significant, *$p < 0.05$, **$p < 0.01$, ***$p < 0.001$, and ****$p < 0.0001$).

stiffness [34,35] and could vary with the polymer MW, DS, and content, as well as the molar ratio between reactive functions. Using compression measurements on 1% (w/v) HA gels at a fixed crosslinking density (1.4 mM) and fixed DS (HA-BCN: 7%; HA-N_3: 40%), we showed that varying HA MW (from 100 to 300 kDa) did not affect stiffness (Fig. 3f), consistent with a previous study [15]. At a fixed crosslinking density (1.4 mM), our results also showed that the stiffness of SPAAC gels is independent of the DS (7% vs 15%) (Fig. 3g). Along with our results on gelation time, these findings suggest that tuning the MW and/or DS of HA is a simple way to tune the gelation time of an HA-based hydrogel without altering its stiffness. Next, we evaluated the influence of the crosslinking density on stiffness by varying the polymer content or the BCN:N_3 molar ratio. As expected, at a fixed MW (100 kDa) and fixed DS (HA-BCN: 15%; HA-N_3: 40%), increasing the polymer content from 0.5% to 1.5% (w/v) in HA gels led to an increase in stiffness from 1.5 ± 0.1 kPa to 6.4 ± 0.5 kPa (Fig. 3h). We further tuned the hydrogel crosslinking density by varying the BCN:N_3 molar ratio. As observed for gelation time, maximizing the crosslinking density by using a BCN:N_3 molar ratio of 1:1 maximized the stiffness of HA gels for a given set of HA precursors; and molar ratios of 4:1, 1:4, and 1:1 led to stiffness values of 0.8 ± 0.1 kPa, 2.7 ± 0.6 kPa, and 4.6 ± 0.2 kPa, respectively (Fig. 3i). We further showed that increasing the crosslinking density, either by increasing the polymer content or tuning the BCN:N_3 molar ratio, increases hydrogel compressive strength (Fig. S2). Markedly, plotting the stiffness of various hydrogel formulations as a function of their crosslinking densities revealed a linear relationship between crosslinking density and stiffness over several orders of magnitude, independently of the MW and DS of HA (Fig. 3j). This relationship allowed us to easily determine the crosslinking density required to produce a gel with a desired stiffness. As a proof of concept, we showed that low MW HA (typically 20 kDa) can be combined with 100 kDa HA to increase the overall polymer content (i.e., the crosslinking density) without affecting the viscosity of the precursor solution, producing HA-based hydrogels with a stiffness (45.3 ± 3.5 kPa) rarely seen before (Fig. S3). In general, using SPAAC as a crosslinking mechanism allowed us to design a new HA-based hydrogel platform with independently controlled gelation time and stiffness suitable to biomedical applications.

3.3. SPAAC hydrogels are stable with tunable swelling behavior

Hydrogel swelling and stability are important parameters to consider for 3D cell culture and tissue engineering purposes. Swelling and shrinking behaviors typically alter the mechanical properties of a gel, thus affecting cell-material interactions. Similarly, an unstable hydrogel

that degrades within hours to days under regular culture conditions is not appropriate for cell culture. Thus, a stable hydrogel with minimal to no swelling/shrinking is desirable. To study the swelling and stability of SPAAC HA gels, we monitored their mass after immersing them in PBS at 37 °C. First, we investigated the role of MW and DS of HA on hydrogel swelling/shrinking. At a fixed crosslinking density (1.4 mM), we observed no difference in swelling/shrinking when varying the MW (100 vs 300 kDa) and DS (HA-BCN: 7% vs 15%) of HA (Fig. 4a,b, and S4a,b), together excluding the contribution of the number of reactive functions per polymer chain to the swelling/shrinking of SPAAC hydrogels.

We then investigated the BCN:N_3 molar ratio at a fixed total HA concentration of 1% or 1.5% (w/v), which resulted in inverted bell curves of shrinking/swelling behavior as a function of the HA content and BCN:N_3 molar ratio. We found that approaching an equimolar ratio of BCN:N_3 led to more shrinking, while extreme BCN:N_3 ratios (i.e., 8:1 and 1:8) led to swelling (Fig. 4c, S4c and S4d). Moreover, increasing the polymer content from 1% to 1.5% (w/v) led to more swelling, no matter the BCN:N_3 molar ratio. We expected this result as HA is a negatively charged and hygroscopic polymer that commonly induces hydrogel swelling in a wet environment due to osmotic pressure [36–38]. Overall, our results demonstrate that the swelling/shrinking behavior of SPAAC HA-based hydrogels depends solely on the HA content and crosslinking density, and finely tuning the crosslinking density for a given HA content can counterbalance osmotic pressure to produce HA gels with the desired swelling/shrinking property. Based on this new understanding,

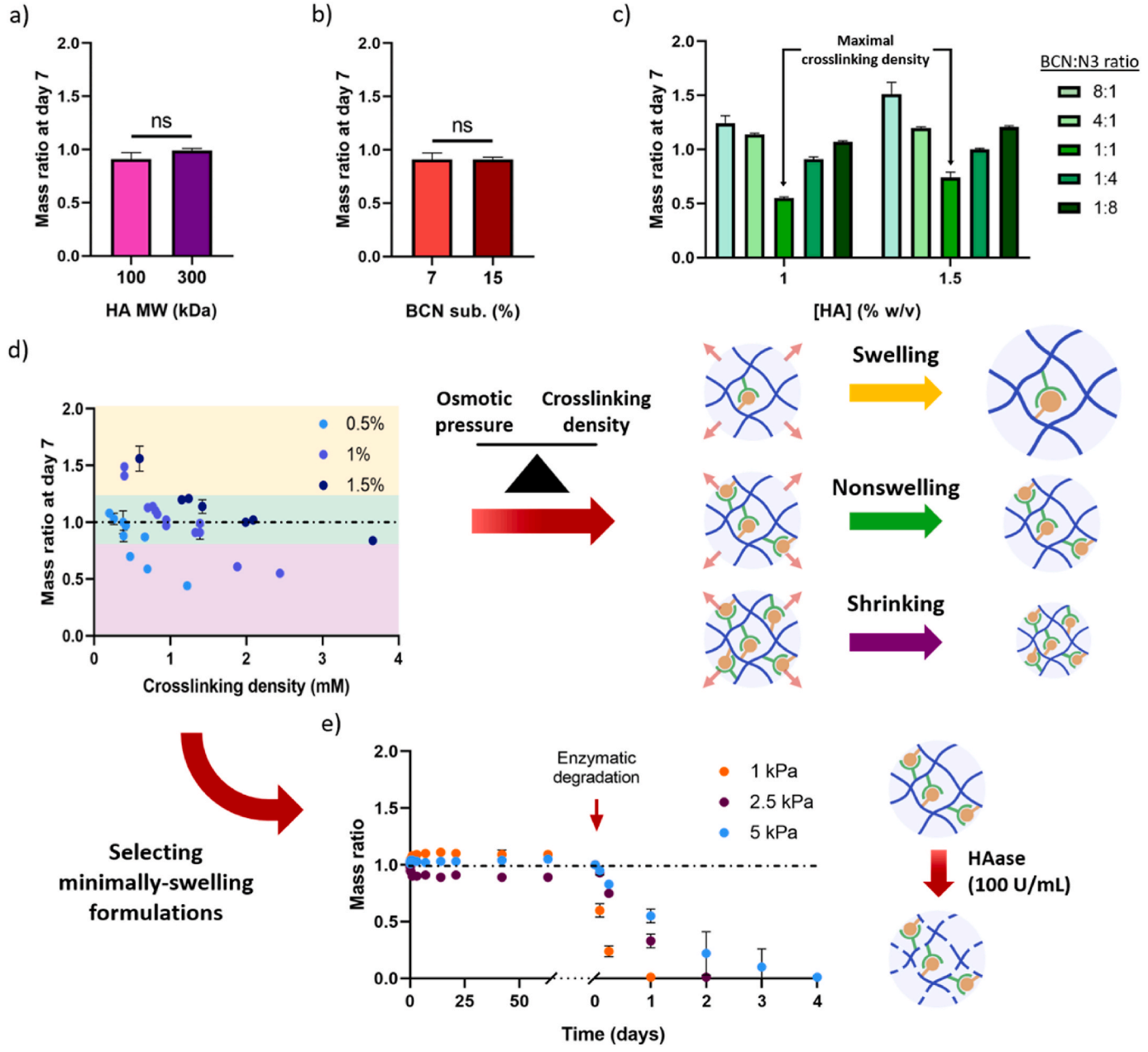

Fig. 4. Stability and swelling characteristics of SPAAC HA-based hydrogels. The influence of a) the MW and b) the BCN substitution of HA on hydrogel mass ratio at day 7. c) The influence of both HA concentration and BCN:N_3 ratio on hydrogel mass ratio at day 7. d) Relationship between hydrogel swelling, hydrogel crosslinking density, and HA concentration, highlighting swelling (yellow arrow), minimally-to non-swelling (green arrow), and shrinking (purple arrow) hydrogel formulations. e) The enzymatic degradation of three SPAAC HA-based hydrogel formulations of interest (stable long term and minimally-to non-swelling with distinct stiffness) using hyaluronidase (100 U mL^{-1}), confirming the biodegradability of the newly designed hydrogels. Data are shown as mean ± SD (n = 3), with statistical significance determined by Student's t-test (ns: not significant).

we identified several formulations for which SPAAC crosslinking density and HA concentration balanced each other to produce minimally-to non-swelling HA-based hydrogels, including some at ultra-low polymer content (0.5% [w/v]) (Fig. 4d).

Most of the SPAAC HA-based hydrogel formulations that we investigated reached their swelling/shrinking equilibrium within 3 days and were then stable over at least 2 months (Fig. S4) while remaining biodegradable under enzymatic degradation (Fig. 4e), making them suitable for long-term cell culture. To date, there has been only one report of stable, minimally-swelling, click and bioorthogonal HA gels [15]. These gels were obtained via inverse electron-demand Diels-Alder crosslinking, which induced the formation of nitrogen bubbles within the gels and produced gels with a low stiffness (≈0.5–3 kPa). In addition, previously reported SPAAC HA-based hydrogels all showed swelling and/or a lack of stability over time [16–18], emphasizing the importance of developing a new hydrogel platform with tunable swelling behavior.

Overall, we demonstrated that SPAAC can serve as an adequate crosslinking strategy to design click and bioorthogonal hydrogels that are easy to synthesize and use. A complete physicochemical characterization of this new system allowed us to obtain a series of HA-based hydrogels that form within minutes, are stable and non-swelling while remaining biodegradable, and offer a range of stiffness suitable to in vitro applications, overcoming the limitations of current hydrogels.

3.4. SPAAC hydrogels are cytocompatible

Conventional crosslinking reactions (e.g., carbodiimide and photocrosslinking) can impair cell viability, limiting their use for 3D cell culture [8,39]. Because of this limitation, developing new click and bioorthogonal crosslinking strategies for cell encapsulation is of particular interest. First, we performed a rheological evaluation of the viscosity of the hydrogel precursors, and showed that the zero-shear viscosity of all of the precursor solutions investigated did not exceed 0.2 Pa s (Fig. S5). These low viscosity profiles confirmed that the hydrogel precursors can be easily mixed together and allow for cell encapsulation. Next, we evaluated the cytocompatibility of SPAAC HA-based hydrogels using a model cell line recommended by ISO10993-5 standards (L929 murine fibroblasts) and hASCs, which are of interest for tissue engineering and cell therapy. A 1% HA hydrogel formulation (DS: HA-BCN: 15%; HA-N_3: 40%; BCN:N_3 ratio of 1:4) with fast gelation (5.6 ± 0.2 min), minimal shrinking, long-term stability, and a stiffness of 2.5 kPa was used to assess the cytocompatibility of the new system. Three distinct polymer batches of HA-BCN and HA-N_3 were used to confirm the safety of the proposed synthetic approach. We first confirmed that these hydrogels displayed similar swelling/stability profiles in PBS and culture medium, and that they showed similar mechanical properties (≈2.5 kPa) either in PBS, culture medium, or in the presence of cells over 7 days of cell culture (Fig. S6). Additional in vitro experiments confirmed the usability of these hydrogels for 3D cell culture experiments of several months (data not shown).

We then assessed cell viability via live/dead staining and confocal microscopy, as well as metabolic activity using a metabolic assay (CCK-8). Encapsulated L929 cells had a cell viability of >95% with no significant change over 7 days (Fig. 5a and b). At day 7, we observed a 7.4 ± 0.6-fold increase of the metabolic activity compared to day 0, consistent with cell proliferation (Fig. 5c), which is common at day 7 of culturing L929 cells [7,40]. In addition, over 7 days of cell culture, encapsulated hASCs were >95% viable (Fig. 5d and e) with constant metabolic activity (Fig. 5f), which is commonly observed with MSCs [41,42]. We did not observe a difference in hASC metabolic activity when immobilizing RGD into the SPAAC hydrogels as an adhesive peptide (Fig. S7), ruling out the effect of a lack of adhesion onto hASC proliferation. Thus, the constant metabolic activity could be due to the lack of a specific stimulus (e.g., proliferation or differentiation medium) in the chosen hASC culture conditions, as well as the cell confinement

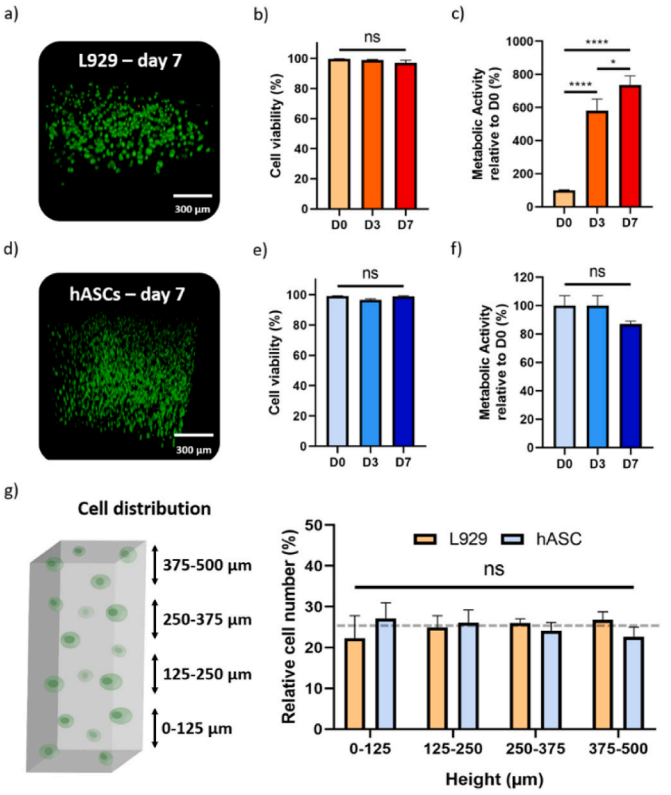

Fig. 5. Cell viability and distribution in SPAAC HA-based hydrogels. a) Representative 3D view, b) cell viability, and c) metabolic activity of encapsulated L929 cells during 7 days of 3D cell culture. d) Representative 3D view, e) cell viability, and f) metabolic activity of encapsulated hASCs during 7 days of 3D cell culture. g) Relative cell distribution within the hydrogel, showing homogenous encapsulation for both cell types used (the dashed line indicates the expected relative cell number in each of the four bins, which is 25%). Data are shown as mean ± SD (n = 3) with statistical significance determined using one-way ANOVA with a Tukey's post hoc test (ns: not significant, *$p < 0.05$ and ****$p < 0.0001$).

[43,44]. Finally, to demonstrate the efficient mixing of cells and hydrogel precursor solutions, we evaluated cell distribution in the 1% HA gels after complete gelation (2 h) using confocal imaging. For both L929 cells and hASCs, the number of cells per volume was not significantly different between hydrogel sections (250 µm), signaling the absence of cell sedimentation and suggesting a homogenous cell distribution throughout the gels (Fig. 5g and h). This finding further confirmed that a gelation time of ≈5–10 min is most appropriate for cell encapsulation and 3D cell culture, as previously suggested [15]. Therefore, our results showed that using SPAAC as a click and bioorthogonal crosslinking strategy facilitates homogeneous and harmless cell encapsulation.

3.5. SPAAC hydrogels allow for straightforward composition modifications

While the role of hydrogel mechanical properties (e.g., stiffness and viscoelasticity) on the behavior of cells has been extensively reviewed [2,45], the roles of biochemical cues remain to be explored. A tunable hydrogel platform that allows for the straightforward incorporation of additional molecules of interest without affecting its mechanical properties would thus facilitate these investigations. Here, we hypothesized that the composition of the new SPAAC hydrogels could be modified via a versatile one-pot procedure in three different ways: first, by replacing HA with another polysaccharide of interest (i.e., polymer switching), such as alginate as a non-bioactive polymer control (Fig. 6a); second, by

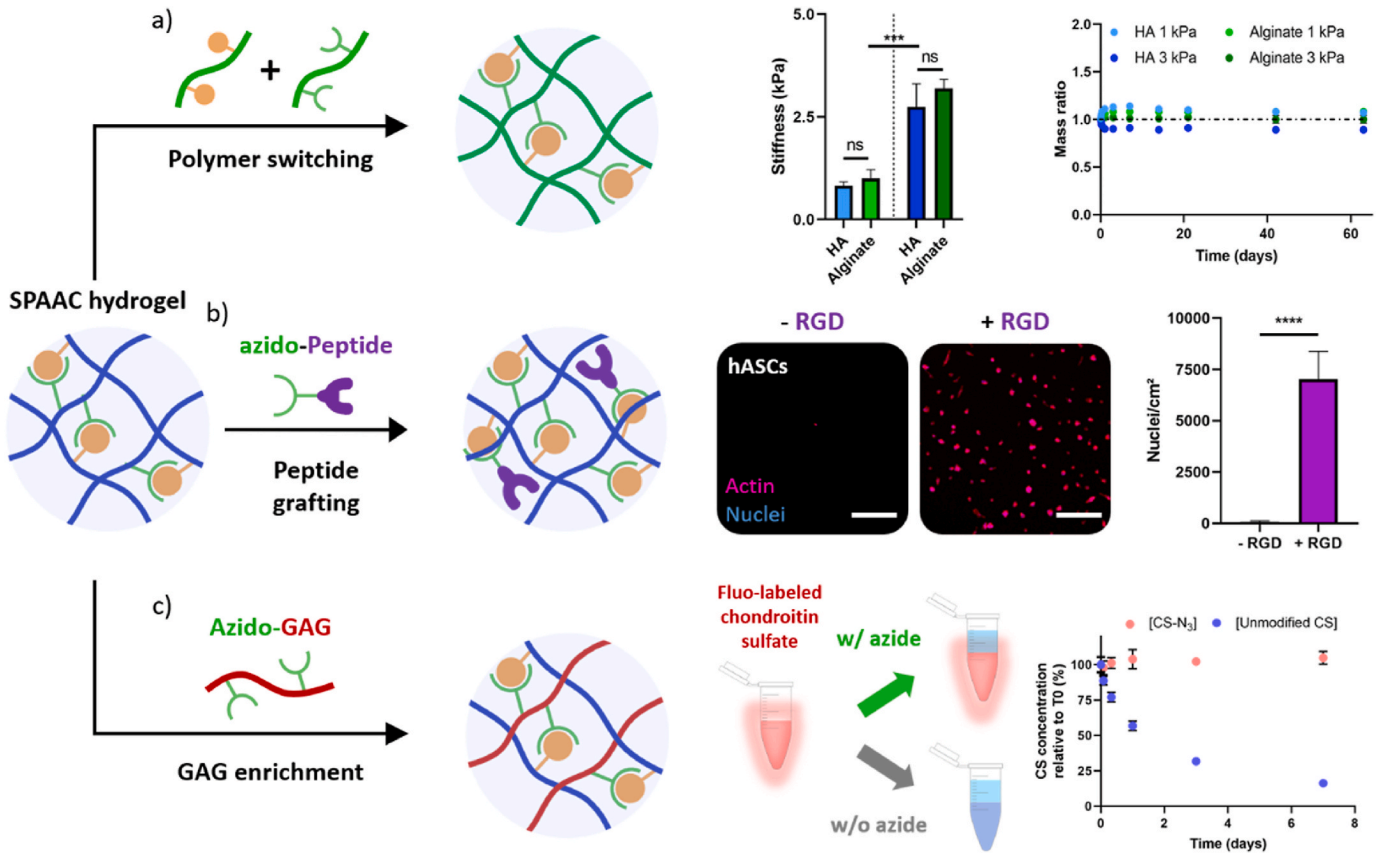

Fig. 6. Versatility of the new SPAAC hydrogel platform with an easily tunable hydrogel composition. a) SPAAC can be applied to other polymers, such as alginate, to obtain hydrogels with similar stiffness and stability but differing in their composition (formulation details can be found in the methods section). b) SPAAC allows peptide grafting to promote cell adhesion, as demonstrated with an azido-RGD peptide immobilization. c) SPAAC facilitates the enrichment of HA hydrogels with other glycosaminoglycans (GAGs), as demonstrated by the monitoring of CS-N_3 retention over 7 days. Data are shown as mean ± SD (n = 3) with statistical significance determined using Student's t-test or one-way ANOVA with a Tukey's post hoc test (ns: not significant, *p < 0.05, **p < 0.01, ***p < 0.001 and ****p < 0.0001).

immobilizing azide-modified biomimetic peptides (i.e., peptide grafting) to promote cell adhesion (Fig. 6b); and third, by co-crosslinking additional glycosaminoglycans (GAG) such as chondroitin sulfate (CS) for GAG enrichment (Fig. 6c).

To investigate polymer switching, we used a synthetic strategy similar to that of SPAAC HA gels to design SPAAC alginate gels by mixing alginate-BCN and alginate-N_3. By optimizing the polymer content, we obtained two alginate hydrogel formulations that were non-swelling and stable for more than 2 months, including after hyaluronidase treatment (Fig. S8), with the same stiffness (1 and 3 kPa) as that of the chosen SPAAC HA hydrogel formulations (Fig. 6a). Being able to modify the polymer backbone of otherwise identical hydrogels (e.g., crosslinking mechanisms, swelling, and mechanical properties) could facilitate future investigations of the effect of individual polymers on cell behavior.

We then investigated the feasibility of incorporating an adhesive peptide (RGD) or of co-crosslinking CS, which have both been shown to play important roles in the regulation of mesenchymal stromal cells (MSC) functions, including MSC secretion and chondrogenesis [46,47]. A commercially available azide-modified RGD peptide (300 μM) was incorporated into a 1% HA gel by simply mixing the peptide solution with one of the two precursors (i.e., HA-BCN) 30 min prior to regular gel formation. This one-pot strategy allowed us to adjust the number of incorporated molecules without an additional synthetic and purification step. To confirm the immobilization and bioactivity of the incorporated adhesive peptide, we assessed 2D cell adhesion using hASCs and cytoskeletal/nuclei (phalloidin/hoechst) staining. After several washes, most cells were washed off in the absence of RGD, whereas immobilizing RGD allowed hASCs to adhere and remain on top of the gel (Fig. 6b). To immobilize CS in SPAAC HA gels, CS was first functionalized with azide functions (CS–N_3) via a similar synthetic procedure to that of HA-N_3. CS-N_3 (0.1%) was then dissolved with HA-N_3 prior to mixing with an HA-BCN solution. To confirm CS co-crosslinking, we compared the release of an azide-modified CS vs unmodified CS from SPAAC HA gels using fluorescently labeled polymers. Monitoring the fluorescence of immersed CS-containing gels, we observed that only the relative amount of incorporated CS-N_3 remained constant over time (104.8% ± 4.6% at day 7), while unmodified CS diffused out of the gel (16.2% ± 1.8% at day 7) (Fig. 6c). These results indicated successful CS co-crosslinking and GAG enrichment. Overall, this one-pot incorporation procedure is broadly applicable to any polymer or peptide and allowed us to further tune the hydrogel composition in a simple way.

3.6. SPAAC HA-based hydrogels influence hASC secretions

MSCs naturally interact with their microenvironment and respond strongly to physical and biochemical variations in their surroundings. But while it may be possible to guide the cell fate or immunomodulatory potential of MSCs by synthetically tuning hydrogels to influence cell-material interactions [3,45], much remains to be done to understand these interactions and their effects on MSC secretory ability. To date, the few studies that have investigated the influence of hydrogel stiffness on MSC immunomodulatory potential showed that soft scaffolds (≤5 kPa) tend to increase MSC secretory ability [48–51]; however, the influence of hydrogel composition on cell secretions remains largely unexplored.

Using our new SPAAC hydrogels, we independently evaluated the

effects of stiffness (1vs 5 kPa), adhesion (RGD vs no RGD), and polymer type (HA vs HA + CS vs alginate) on MSCs' ability to secrete immunomodulatory factors in response to a pro-inflammatory environment. Specifically, hASCs were encapsulated in our different hydrogels and cultured under pro-inflammatory conditions (TNF-α and INF-γ) for 3 days. We then analyzed the supernatants to quantify the presence of three soluble factors known to mitigate inflammation: indoleamine 2,3-dioxygenase (IDO), prostaglandin E2 (PGE2), and interleukin-6 (IL-6) (Fig. 7a) [23,52]. Our results showed that IDO activity (tryptophan-to-kynurenine conversion) and PGE2 and IL-6 levels were consistent across our different hydrogels, suggesting that tuning HA hydrogel stiffness (1 vs 5 kPa) or enriching gels with CS did not affect hASC secretions (Fig. 7b, c, and d). This is the first report of the potential lack of effect of CS enrichment on hASC paracrine functions. Regarding the effect of changes in stiffness, our results are consistent with a previous study that showed that varying the shear elastic modulus of covalently crosslinked hydrogels between 0.25 kPa and 2.5 kPa did not affect the secretion of PGE2 by encapsulated MSCs [53].

Regarding adhesion, our data showed that the chemical immobilization of the adhesive RGD peptide to a soft HA hydrogel (1 kPa) did not significantly alter the secretion of IDO and IL-6 by the encapsulated MSCs (Fig. 7b, d); however, immobilizing RGD did decrease the secretion of PGE2 (3.16 ± 0.48 ng/mL vs 6.28 ± 0.94 ng/mL) (Fig. 7c). Our finding that RGD did not alter IL-6 secretion is consistent with another study, where the encapsulation of MSCs in a PEG hydrogel containing RGD vs a non-adhesive scrambled control (RDG) did not lead to significant differences in the secretion of IL-6, IL-8, and VEGF [54]. Moreover, the observed reduced secretion of PGE2 may have resulted from an early stage of cell differentiation triggered by cell adhesion, as differentiated cells are known to secrete fewer immunomodulatory factors than undifferentiated MSCs [55]. The reduction of PGE2 could also have been the result of decreased stress due to adhesion to the matrix, as stress has been previously correlated with increased PGE2 secretion via the NF-κB pathway [56].

Interestingly, compared to a HA hydrogel control, when hASCs were encapsulated in a SPAAC alginate hydrogel (1 kPa), the supernatant showed significantly reduced IDO activity (55.47 ± 4.2 μM vs 77.58 ± 2.81 μM) and significantly reduced levels of PGE2 (2.4 ± 1.2 ng/mL vs 6.28 ± 0.94 ng/mL) and IL-6 (17.11 ± 3.34 ng/mL vs 24.74 ± 1.43 ng/mL). While we could not fully exclude distinct diffusion properties, the two hydrogels had similar mechanical properties with similar crosslinking densities, suggesting that the altered secretion in alginate gels may be the result of distinct polymer structures and cell-material interactions. Unlike alginate, HA is a bioactive polymer and is known to interact with cells through receptors such as CD44 and RHAMM [5,57]. While HA is most often considered and used as a polymer of interest for its biological relevance, this is the first time an HA gel has been reported to have a positive effect on MSC secretions based on a direct comparison to a non-HA-based hydrogel. While beyond the scope of this article, our results call for further investigations of potential pathways activated by HA, possibly leading to tailored HA-based materials for improved biomedical applications, such as stem cell therapy. Conversely to the use of HA, the incorporation of CS to the SPAAC hydrogels had no effect on the secretion of IDO, PGE2, and IL-6. A previous study showed that incorporating CS into scaffolds could increase the production of NO and PGE2 by MSCs [58]. However, this was demonstrated using collagen-based scaffolds with a stiffness higher by several orders of magnitude, where cells were seeded onto the scaffolds. The differences in culture conditions (2D vs 3D), polymer composition and stiffness could explain the divergent results. Overall, the versatility of our new SPAAC hydrogel platform, where composition and stiffness can be easily adjusted without compromising gelation time and stability, has provided us with a new avenue to investigate cell-material interactions.

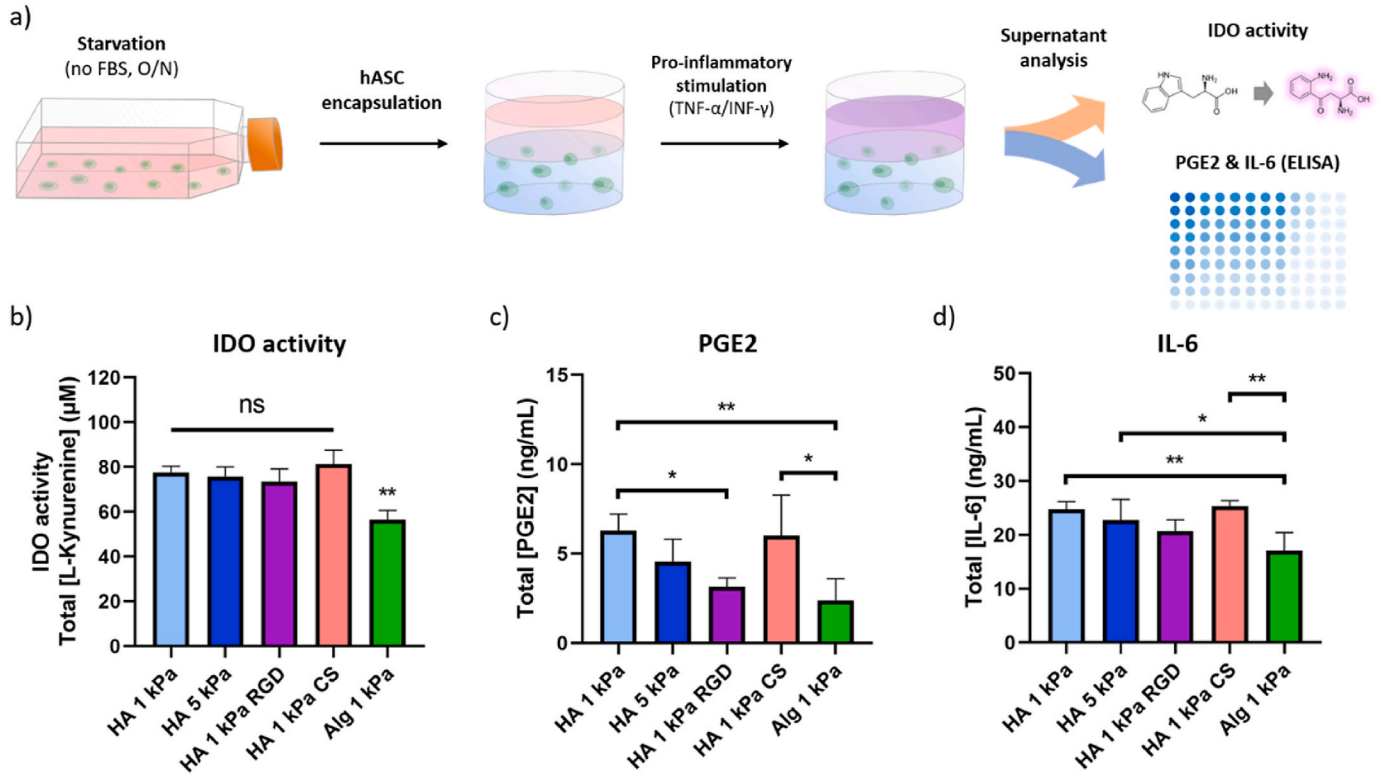

Fig. 7. The ultra-tunable SPAAC hydrogel platform revealed that HA has a positive effect on encapsulated MSC secretions, while CS has no effect. a) Schematic of the procedure: hASCs are deprived of FBS overnight prior to being encapsulated in hydrogels and stimulated with pro-inflammatory cytokines (TNF-α and INF-γ). After 3 days, the supernatant is collected to evaluate b) the presence of IDO via its enzymatic activity, and the levels of c) PGE2 and d) IL-6. Data are shown as mean ± SD (n = 4), with statistical significance determined using one-way ANOVA with a Tukey's post hoc test (ns: not significant, *p < 0.05, **p < 0.01).

4. Conclusion

Using SPAAC as a click and bioorthogonal crosslinking strategy, we successfully developed a practical and easily tunable HA-based hydrogel platform. Our unique hydrogels are easy to synthesize and sterilize, have a controlled gelation rate and long-term stability with minimal swelling, are cytocompatible, and are ultra-tunable in terms of mechanical properties (i.e., stiffness ranging at least 2 orders of magnitude) and biochemical properties (i.e., polymer composition and adhesion). As such, these hydrogels can easily be tailored for a variety of biomedical applications and translational research, including 3D cell culture to investigate cell-material interactions. Using this new platform, we demonstrated for the first time that HA can enhance the secretion of immunomodulatory factors by encapsulated hASCs, potentially laying the foundation for a new generation of material-assisted cell therapies.

Ethics approval and consent to participate

This manuscript has not been previously published by any of the authors and is not currently under consideration in another journal. All authors have seen and approved this submission.

CRediT authorship contribution statement

Nathan Lagneau: Conceptualization, Methodology, Investigation, Data curation, Formal analysis, Writing - original draft. **Pierre Tournier:** Investigation, Conceptualization, Methodology. **Boris Halgand:** Resources. **François Loll:** Resources. **Yves Maugars:** Supervision. **Jérôme Guicheux:** Supervision, Writing - review & editing. **Catherine Le Visage:** Writing – review & editing, Supervision. **Vianney Delplace:** Conceptualization, Methodology, Supervision, Project administration, Validation, Writing - original draft, Writing - review & editing.

Declaration of competing interest

The authors declare no conflict of interest.

Acknowledgments

The authors are grateful to the Fondation de l'Avenir pour la Recherche Médicale Appliquée (AP-RM-18-005; CLV), the Fondation pour la Recherche Médicale (ARF201809007012; VD), the Nantes Excellence Trajectory program (NExT Junior Talent 2018, VD; NexT IIP Shelby 2018, CLV), and the Marie-Sklodowska Curie Actions (BABHY-CART project, GAP-846477; VD) for their financial support. They also thank the MicroPICell facility (Nantes, FRANCE) and Virginie Silvestre at the CEISAM NMR platform (Nantes, FRANCE) for their technical support in confocal microscopy and NMR, respectively. The authors wish to thank Miriam Bergeret for editing the manuscript.

Appendix A. Supplementary data

Supplementary data to this article can be found online at https://doi.org/10.1016/j.bioactmat.2022.12.022.

References

[1] J. Lee, O. Jeon, M. Kong, A.A. Abdeen, J.-Y. Shin, H.N. Lee, Y. Bin Lee, W. Sun, P. Bandaru, D.S. Alt, K. Lee, H. Kim, S.J. Lee, S. Chaterji, S.R. Shin, E. Alsberg, A. Khademhosseini, Combinatorial screening of biochemical and physical signals for phenotypic regulation of stem cell–based cartilage tissue engineering, Sci. Adv. 6 (2020), eaaz5913, https://doi.org/10.1126/sciadv.aaz5913.

[2] N. Huebsch, P.R. Arany, A.S. Mao, D. Shvartsman, O.A. Ali, S.A. Bencherif, D. J. Mooney, Harnessing traction-mediated manipulation of the cell-matrix interface to control stem cell fate, Nat. Mater. 9 (2010) 518–526, https://doi.org/10.1038/nmat2732.

[3] C.M. Madl, S.C. Heilshorn, Engineering hydrogel microenvironments to recapitulate the stem cell niche, Annu. Rev. Biomed. Eng. 20 (2018) 21–47, https://doi.org/10.1146/annurev-bioeng-062117-120954.

[4] J.A. Burdick, G.D. Prestwich, Hyaluronic acid hydrogels for biomedical applications, Adv. Mater. 23 (2011) 41–56, https://doi.org/10.1002/adma.201003963.

[5] A. Aruffo, I. Stamenkovic, M. Melnick, C.B. Underhill, B. Seed, CD44 is the principal cell surface receptor for hyaluronate, Cell 61 (1990) 1303–1313, https://doi.org/10.1016/0092-8674(90)90694-A.

[6] C. Loebel, C.B. Rodell, M.H. Chen, J.A. Burdick, Shear-thinning and self-healing hydrogels as injectable therapeutics and for 3D-printing, Nat. Protoc. 12 (2017) 1521–1541, https://doi.org/10.1038/nprot.2017.053.

[7] K. Flegeau, C. Toquet, G. Rethore, C. d'Arros, L. Messager, B. Halgand, D. Dupont, F. Autrusseau, J. Lesoeur, J. Veziers, P. Bordat, A. Bresin, J. Guicheux, V. Delplace, H. Gautier, P. Weiss, In situ forming, silanized hyaluronic acid hydrogels with fine control over mechanical properties and in vivo degradation for tissue engineering applications, Adv. Healthc. Mater. 9 (2020) 1–11, https://doi.org/10.1002/adhm.202000981.

[8] N.E. Fedorovich, M.H. Oudshoorn, D. van Geemen, W.E. Hennink, J. Alblas, W.J. A. Dhert, The effect of photopolymerization on stem cells embedded in hydrogels, Biomaterials 30 (2009) 344–353, https://doi.org/10.1016/j.biomaterials.2008.09.037.

[9] C.M. Madl, S.C. Heilshorn, Rapid diels-alder cross-linking of cell encapsulating hydrogels, Chem. Mater. 31 (2019) 8035–8043, https://doi.org/10.1021/acs.chemmater.9b02485.

[10] H.C. Kolb, M.G. Finn, K.B. Sharpless, Click chemistry: diverse chemical function from a few good reactions, Angew. Chem. Int. Ed. 40 (2001) 2004–2021, https://doi.org/10.1002/1521-3773(20010601)40:11<2004::AID-ANIE2004>3.0.CO.

[11] E.M. Sletten, C.R. Bertozzi, From mechanism to mouse: a tale of two bioorthogonal reactions, Acc. Chem. Res. 44 (2011) 666–676, https://doi.org/10.1021/ar200148z.

[12] S.L. Scinto, D.A. Bilodeau, R. Hincapie, W. Lee, S.S. Nguyen, M. Xu, C.W. am Ende, M.G. Finn, K. Lang, Q. Lin, J.P. Pezacki, J.A. Prescher, M.S. Robillard, J.M. Fox, Bioorthogonal chemistry, Nat. Rev. Methods Prim. 1 (2021) 1–30, https://doi.org/10.1038/s43586-021-00028-z.

[13] C.M. Madl, S.C. Heilshorn, Bioorthogonal strategies for engineering extracellular matrices, Adv. Funct. Mater. 28 (2018) 1706046–1706067, https://doi.org/10.1002/adfm.201706046.

[14] H. Tan, J.P. Rubin, K.G. Marra, Direct synthesis of biodegradable polysaccharide derivative hydrogels through aqueous Diels-Alder chemistry, Macromol. Rapid Commun. 32 (2011) 905–911, https://doi.org/10.1002/marc.201100125.

[15] V. Delplace, P.E.B. Nickerson, A. Ortin-Martinez, A.E.G. Baker, V.A. Wallace, M. S. Shoichet, Nonswelling, ultralow content inverse electron-demand diels–alder hyaluronan hydrogels with tunable gelation time: synthesis and in vitro evaluation, Adv. Funct. Mater. 30 (2020) 1–11, https://doi.org/10.1002/adfm.201903978.

[16] A. Takahashi, Y. Suzuki, T. Suhara, K. Omichi, A. Shimizu, K. Hasegawa, N. Kokudo, S. Ohta, T. Ito, In situ cross-linkable hydrogel of hyaluronan produced via copper-free click chemistry, Biomacromolecules 14 (2013) 3581–3588, https://doi.org/10.1021/bm4009606.

[17] S.S. Han, H.Y. Yoon, J.Y. Yhee, M.O. Cho, H.E. Shim, J.E. Jeong, D.E. Lee, K. Kim, H. Guim, J.H. Lee, K.M. Huh, S.W. Kang, In situ cross-linkable hyaluronic acid hydrogels using copper free click chemistry for cartilage tissue engineering, Polym. Chem. 9 (2018) 20–27, https://doi.org/10.1039/c7py01654a.

[18] S. Fu, H. Dong, X. Deng, R. Zhuo, Z. Zhong, Injectable hyaluronic acid/poly (ethylene glycol) hydrogels crosslinked via strain-promoted azide-alkyne cycloaddition click reaction, Carbohydr. Polym. 169 (2017) 332–340, https://doi.org/10.1016/j.carbpol.2017.04.028.

[19] J. Christoffersson, C. Aronsson, M. Jury, R. Selegård, D. Aili, C.F. Mandenius, Fabrication of modular hyaluronan-PEG hydrogels to support 3D cultures of hepatocytes in a perfused liver-on-a-chip device, Biofabrication 11 (2019), https://doi.org/10.1088/1758-5090/aaf657.

[20] S.M. Hull, C.D. Lindsay, L.G. Brunel, D.J. Shiwarski, J.W. Tashman, J.G. Roth, D. Myung, A.W. Feinberg, S.C. Heilshorn, 3D bioprinting using UNIversal orthogonal network (UNION) bioinks, Adv. Funct. Mater. 31 (2021), 2007983, https://doi.org/10.1002/adfm.202007983.

[21] C.T. Moody, S. Palvai, Y. Brudno, Click cross-linking improves retention and targeting of refillable alginate depots, Acta Biomater. 112 (2020) 112–121, https://doi.org/10.1016/j.actbio.2020.05.033.

[22] M. Nouri-Felekori, N. Nezafati, M. Moraveji, S. Hesaraki, T. Ramezani, Bioorthogonal hydroxyethyl cellulose-based scaffold crosslinked via click chemistry for cartilage tissue engineering applications, Int. J. Biol. Macromol. 183 (2021) 2030–2043, https://doi.org/10.1016/j.ijbiomac.2021.06.005.

[23] N. Song, M. Scholtemeijer, K. Shah, Mesenchymal stem cell immunomodulation: mechanisms and therapeutic potential, Trends Pharmacol. Sci. 41 (2020) 653–664, https://doi.org/10.1016/j.tips.2020.06.009.

[24] Y. Shi, Y. Wang, Q. Li, K. Liu, J. Hou, C. Shao, Y. Wang, Immunoregulatory mechanisms of mesenchymal stem and stromal cells in inflammatory diseases, Nat. Rev. Nephrol. 14 (2018) 493–507, https://doi.org/10.1038/s41581-018-0023-5.

[25] C. Merceron, S. Portron, C. Vignes-Colombeix, E. Rederstorff, M. Masson, J. Lesoeur, S. Sourice, C. Sinquin, S. Colliec-Jouault, P. Weiss, C. Vinatier, J. Guicheux, Pharmacological modulation of human mesenchymal stem cell chondrogenesis by a chemically oversulfated polysaccharide of marine origin: potential application to cartilage regenerative medicine, Stem Cell. 30 (2012) 471–480, https://doi.org/10.1002/stem.1686.

[26] F. Hached, C. Vinatier, P.G. Pinta, P. Hulin, C. Le Visage, P. Weiss, J. Guicheux, A. Billon-Chabaud, G. Grimandi, Polysaccharide hydrogels support the long-Term

viability of encapsulated human mesenchymal stem cells and their ability to secrete immunomodulatory factors, Stem Cell. Int. 2017 (2017) 6–8, https://doi.org/10.1155/2017/9303598.
[27] J. Dommerholt, F.P.J.T. Rutjes, F.L. van Delft, Strain-promoted 1,3-dipolar cycloaddition of cycloalkynes and organic azides, Top. Curr. Chem. 374 (2016) 1–20, https://doi.org/10.1007/s41061-016-0016-4.
[28] R. Selegård, C. Aronsson, C. Brommesson, S. Dånmark, D. Aili, Folding driven self-assembly of a stimuli-responsive peptide-hyaluronan hybrid hydrogel, Sci. Rep. 7 (2017) 1–9, https://doi.org/10.1038/s41598-017-06457-9.
[29] W.H. Stockmayer, Theory of molecular size distribution and gel formation in branched polymers: II. General cross linking, J. Chem. Phys. 12 (1944) 125–131, https://doi.org/10.1063/1.1723922.
[30] K.S. Anseth, C.N. Bowman, Kinetic Gelation model predictions of crosslinked polymer network microstructure, Chem. Eng. Sci. 49 (1994) 2207–2217, https://doi.org/10.1016/0009-2509(94)E0055-U.
[31] A.L. Kjøniksen, B. Nyström, Effects of polymer concentration and cross-linking density on rheology of chemically cross-linked poly(vinyl alcohol) near the gelation threshold, Macromolecules 29 (1996) 5215–5222, https://doi.org/10.1021/ma960094q.
[32] W. Cao, J. Sui, M. Ma, Y. Xu, W. Lin, Y. Chen, Y. Man, Y. Sun, Y. Fan, X. Zhang, The preparation and biocompatible evaluation of injectable dual crosslinking hyaluronic acid hydrogels as cytoprotective agents, J. Mater. Chem. B. 7 (2019) 4413–4423, https://doi.org/10.1039/c9tb00839j.
[33] A.J. Engler, S. Sen, H.L. Sweeney, D.E. Discher, Matrix elasticity directs stem cell lineage specification, Cell 126 (2006) 677–689, https://doi.org/10.1016/j.cell.2006.06.044.
[34] S. Lin, L. Gu, Influence of crosslink density and stiffness on mechanical properties of type I collagen gel, Materials (Basel) 8 (2015) 551–560, https://doi.org/10.3390/ma8020551.
[35] K. Kato, Y. Ikeda, K. Ito, Direct determination of cross-link density and its correlation with the elastic modulus of a gel with slidable cross-links, ACS Macro Lett. 8 (2019) 700–704, https://doi.org/10.1021/acsmacrolett.9b00238.
[36] C.B. Rodell, N. Dusaj, C.B. Highley, J.A. Burdick, Injectable and cytocompatible tough double network hydrogels through tandem supramolecular and covalent crosslinking, Adv. Mater. 28 (2016) 8419–8424, https://doi.org/10.1002/adma.201602268.Injectable.
[37] X.Z. Shu, Y. Liu, Y. Luo, M.C. Roberts, G.D. Prestwich, Disulfide cross-linked hyaluronan hydrogels, Biomacromolecules 3 (2002) 1304–1311, https://doi.org/10.1021/bm025603c.
[38] L.J. Smith, S.M. Taimoory, R.Y. Tam, A.E.G. Baker, N. Binth Mohammad, J. F. Trant, M.S. Shoichet, Diels-alder click-cross-linked hydrogels with increased reactivity enable 3D cell encapsulation, Biomacromolecules 19 (2018) 926–935, https://doi.org/10.1021/acs.biomac.7b01715.
[39] J.Y. Lai, Biocompatibility of chemically cross-linked gelatin hydrogels for ophthalmic use, J. Mater. Sci. Mater. Med. 21 (2010) 1899–1911, https://doi.org/10.1007/s10856-010-4035-3.
[40] A. Blaeser, D.F. Duarte Campos, M. Weber, S. Neuss, B. Theek, H. Fischer, W. Jahnen-Dechent, Biofabrication under fluorocarbon: a novel freeform fabrication technique to generate high aspect ratio tissue-engineered constructs, Biores. Open Access 2 (2013) 374–384, https://doi.org/10.1089/biores.2013.0031.
[41] Y. Dong, Y. Liu, Y. Chen, X. Sun, L. Zhang, Z. Zhang, Y. Wang, C. Qi, S. Wang, Q. Yang, Spatiotemporal regulation of endogenous MSCs using a functional injectable hydrogel system for cartilage regeneration, NPG Asia Mater. 13 (2021) 71, https://doi.org/10.1038/s41427-021-00339-3 NPG.
[42] K. Flegeau, O. Gauthier, G. Rethore, F. Autrusseau, A. Schaefer, J. Lesoeur, J. Veziers, A. Brésin, H. Gautier, P. Weiss, Injectable silanized hyaluronic acid hydrogel/biphasic calcium phosphate granule composites with improved handling and biodegradability promote bone regeneration in rabbits, Biomater. Sci. 9 (2021) 5640–5651, https://doi.org/10.1039/d1bm00403d.
[43] S. Nam, V.K. Gupta, H. Lee, J.Y. Lee, K.M. Wisdom, S. Varma, E.M. Flaum, C. Davis, R.B. West, O. Chaudhuri, Cell cycle progression in confining microenvironments is regulated by a growth-responsive TRPV4-PI3K/Akt-p27 Kip1 signaling axis, Sci. Adv. 5 (2019), https://doi.org/10.1126/sciadv.aaw6171.
[44] O.Y. Dudaryeva, A. Bucciarelli, G. Bovone, F. Huwyler, S. Jaydev, N. Broguiere, M. Al-Bayati, M. Lütolf, M.W. Tibbitt, 3D confinement regulates cell life and death, Adv. Funct. Mater. 31 (2021), 2104098, https://doi.org/10.1002/adfm.202104098.
[45] O. Chaudhuri, J. Cooper-White, P.A. Janmey, D.J. Mooney, V.B. Shenoy, Effects of extracellular matrix viscoelasticity on cellular behaviour, Nature 584 (2020) 535–546, https://doi.org/10.1038/s41586-020-2612-2.
[46] S.S. Ho, K.C. Murphy, B.Y.K. Binder, C.B. Vissers, J.K. Leach, Increased survival and function of mesenchymal stem cell spheroids entrapped in instructive alginate hydrogels, Stem Cells Transl. Med. 5 (2016) 773–781, https://doi.org/10.5966/sctm.2015-0211.
[47] E.A. Aisenbrey, S.J. Bryant, The role of chondroitin sulfate in regulating hypertrophy during MSC chondrogenesis in a cartilage mimetic hydrogel under dynamic loading, Biomaterials 190–191 (2019) 51–62, https://doi.org/10.1016/j.biomaterials.2018.10.028.
[48] Y. Ji, J. Li, Y. Wei, W. Gao, X. Fu, Y. Wang, Substrate stiffness affects the immunosuppressive and trophic function of hMSCs: via modulating cytoskeletal polymerization and tension, Biomater. Sci. 7 (2019) 5292–5300, https://doi.org/10.1039/c9bm01202h.
[49] H. Yang, N.M.J. Cheam, H. Cao, M.K.H. Lee, S.K. Sze, N.S. Tan, C.Y. Tay, Materials stiffness-dependent redox metabolic reprogramming of mesenchymal stem cells for secretome-based therapeutic angiogenesis, Adv. Healthc. Mater. 8 (2019), e1900929, https://doi.org/10.1002/adhm.201900929.
[50] K.C. Murphy, J. Whitehead, D. Zhou, S.S. Ho, J.K. Leach, Engineering fibrin hydrogels to promote the wound healing potential of mesenchymal stem cell spheroids, Acta Biomater. 64 (2017) 176–186, https://doi.org/10.1016/j.actbio.2017.10.007.
[51] S.W. Wong, S. Lenzini, M.H. Cooper, D.J. Mooney, J.W. Shin, Soft extracellular matrix enhances inflammatory activation of mesenchymal stromal cells to induce monocyte production and trafficking, Sci. Adv. 6 (2020) aaw0158, https://doi.org/10.1126/sciadv.aaw0158.
[52] X. Zhao, Y. Zhao, X. Sun, Y. Xing, X. Wang, Q. Yang, Immunomodulation of MSCs and MSC-derived extracellular vesicles in osteoarthritis, Front. Bioeng. Biotechnol. 8 (2020) 1–14, https://doi.org/10.3389/fbioe.2020.575057.
[53] K.H. Vining, A. Stafford, D.J. Mooney, Sequential modes of crosslinking tune viscoelasticity of cell-instructive hydrogels, Biomaterials 188 (2019) 187–197, https://doi.org/10.1016/j.biomaterials.2018.10.013.
[54] A.Y. Clark, K.E. Martin, J.R. García, C.T. Johnson, H.S. Theriault, W.M. Han, D. W. Zhou, E.A. Botchwey, A.J. García, Integrin-specific hydrogels modulate transplanted human bone marrow-derived mesenchymal stem cell survival, engraftment, and reparative activities, Nat. Commun. 11 (2020) 114, https://doi.org/10.1038/s41467-019-14000-9.
[55] Y. Park, C. Ha, J. Kim, Comparison of undifferentiated versus chondrogenic predifferentiated mesenchymal stem cells derived from human umbilical cord blood for cartilage repair in a rat model, Am. J. Sports Med. 47 (2019) 451–461.
[56] J. Ylöstalo, T. Bartosh, K. Coble, D. Prockop, Human mesenchymal stem/stromal cells (hMSCs) cultured as spheroids are self-activated to produce prostaglandin E2 (PGE2) that directs stimulated macrophages into an anti-inflammatory phenotype, Stem Cell. 30 (2012) 2283–2296, https://doi.org/10.1002/stem.1191.
[57] S. Misra, V. Hascall, R. Markwald, S. Ghatak, Interactions between hyaluronan and its receptors (CD44 , RHAMM) regulate the activities of, Front. Immunol. 6 (2015) 201, https://doi.org/10.3389/fimmu.2015.00201.
[58] B. Corradetti, F. Taraballi, S. Minardi, J. Van Eps, F. Cabrera, L.W. Francis, S. A. Gazze, M. Ferrari, B.K. Weiner, E. Tasciotti, Chondroitin sulfate immobilized on a biomimetic scaffold modulates inflammation while driving chondrogenesis, Stem Cells Transl. Med. 5 (2016) 670–682, https://doi.org/10.5966/sctm.2015-0233.